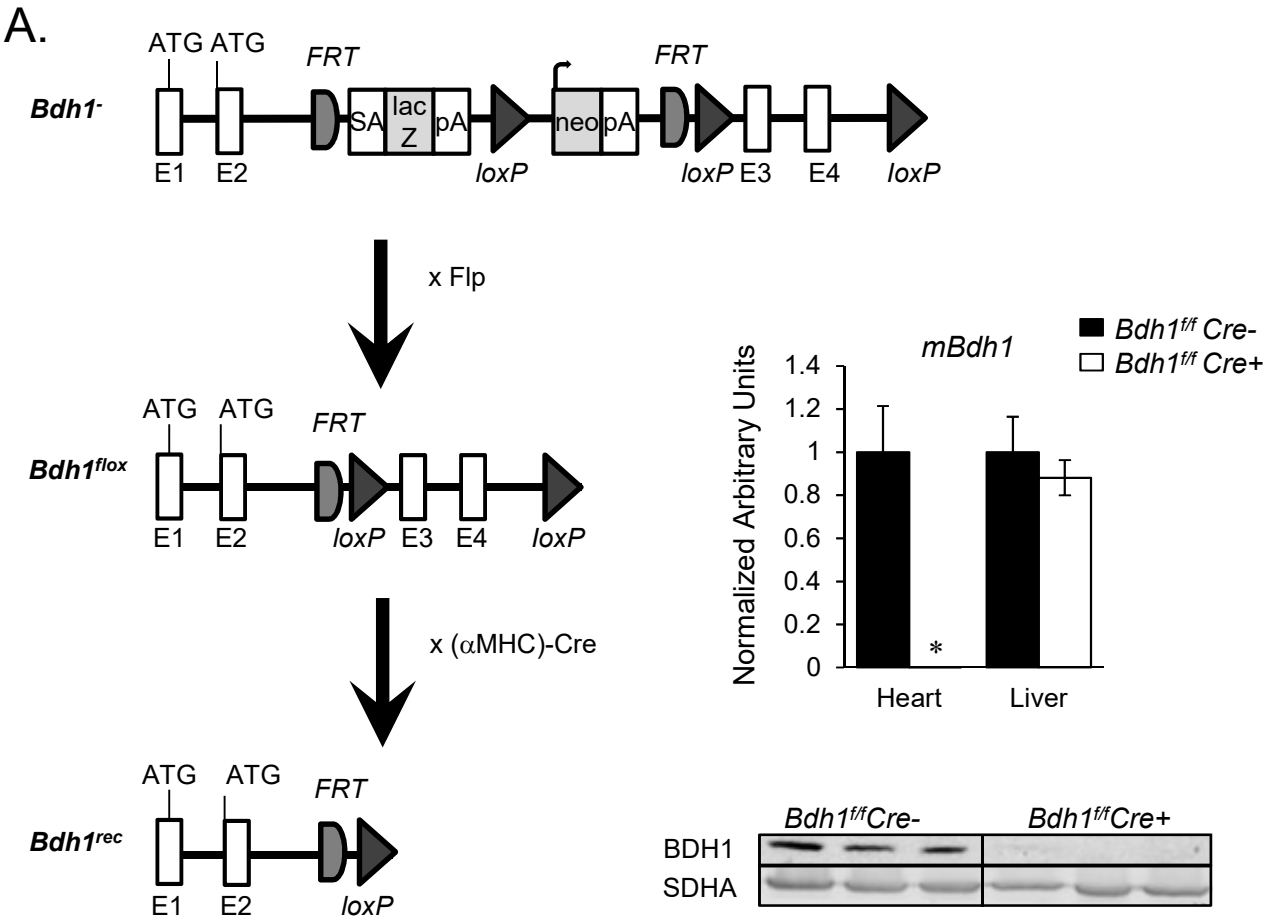
A.
ATG ATG
FRT
FRT
Bdh1-
SA
lac Z
pA
neo
pA
E1
E2
loxP
loxP
E3
E4
loxP
x Flp
Bdh1flox
ATG ATG
FRT
E1
E2
loxP
E3
E4
loxP
x (αMHC)-Cre
Bdh1rec
ATG ATG
FRT
E1
E2
loxP
mBdh1
Bdh1f/f Cre-
Bdh1f/f Cre+
Normalized Arbitrary Units
1.4
1.2
1
0.8
0.6
0.4
0.2
0
*
Heart
Liver
Bdh1f/fCre-
Bdh1f/fCre+
BDH1
SDHA

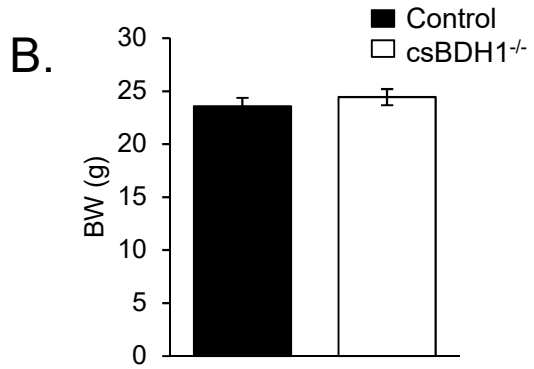
B.
Control
csBDH1-/-
BW (g)
30
25
20
15
10
5
0

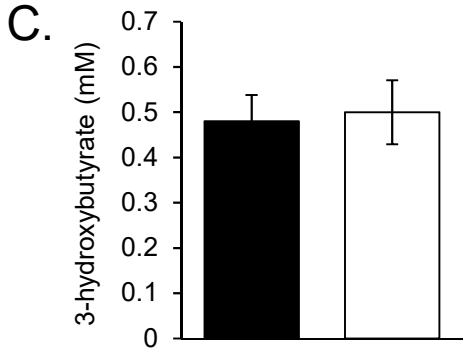
C.
3-hydroxybutyrate (mM)
0.7
0.6
0.5
0.4
0.3
0.2
0.1
0

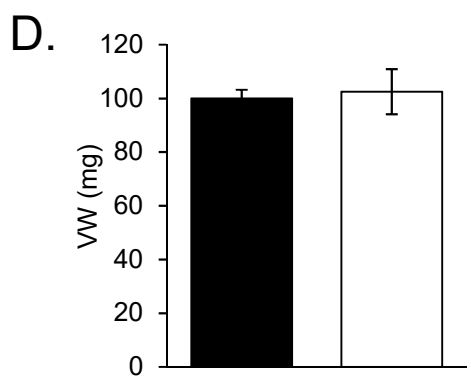
D.
VW (mg)
120
100
80
60
40
20
0

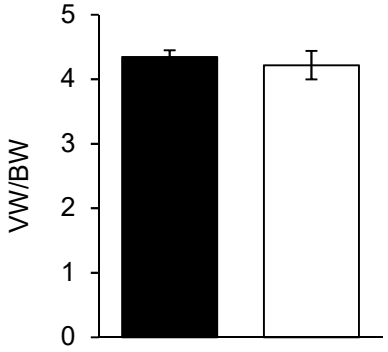
VW/BW
5
4
3
2
1
0

Supplemental Figure 1. Generation and baseline characterization of the csBDH1$^{-/-}$ mouse line. (A, Schematic) Strategy used to generate csBDH1$^{-/-}$ mice. ES cells harboring Bdh1 targeting (Bdh1^{-}) constructed alleles (top row) were injected into blastocysts for creation of founder mice. Start codons for transcript variants of *Bdh1* are indicated by ATG. Loxp sites flanked exons 3 and 4 (exons 5-7 in construct but not shown). Pairing with Flp mice produced offspring harboring *Bdh1*^{flox} alleles. *Bdh1*$_{flox}$ mice were then mated with α*MHC-Cre*$^{+/-}$ mice. The *Bdh1*^{rec} diagram (bottom row) shows the recombined *Bdh1* allele. **(A, Bar graph)** *Bdh1* mRNA in heart and liver tissue of *Cre*$^{-/-}$, *Bdh1*$^{f/f}$ and *Cre*$^{-/+}$, *Bdh1*$^{f/f}$ mice. Expression corrected to *Rplp0* and normalized to Cre$^{-/-}$, Bdh1$^{f/f}$ (=1). Bars represent mean ± SEM (n = 3-6); *p-value<0.05 using two-tailed, unpaired Welch's t-test heart *Bdh1*$^{f/f}$*Cre*$^{-}$ vs. *Bdh1*$^{f/f}$ *Cre*$^{+}$ or two-tailed, unpaired t-test liver *Bdh1*$^{f/f}$*Cre*$^{-}$ vs. *Bdh1*$^{f/f}$ *Cre*$^{+}$. (**A, western blot**) Representative western blot analysis (bottom) using protein lysate from hearts of *Bdh1*$^{f/f}$*Cre*$^{-}$ or *Bdh1*$^{f/f}$ *Cre*$^{+}$ mice (n=3). Antibodies used are labeled on the left. Anti-SDHA was used as a mitochondrial protein-loading control. Cs, cardiac specific; BDH1, 3-hydroxybutyrate dehydrogenase, type 1 ;ES, embryonic stem; FRT, flippase recognition target; SA, splice acceptor; lacZ, β-galactosidase gene; neo, neomycin resistance gene; pA, poly-A; loxp, Locus of Crossover in P1; Flp, Flp1 recombinase; αMHC, myosin heavy chain, a isoform; rec, recombined; Rplp0, Ribosomal Protein Lateral Stalk Subunit P0; SDHA, succinate dehydrogenase, subunit A. **(B)** Body weight of control and csBDH1$^{-/-}$ male mice littermates at 8-12 weeks of age. Bars represent mean ± SEM (n = 9-10); not significant using two-tailed, unpaired Mann-Whitney test control vs. csBDH1$^{-/-}$. **(C)** Circulating 3-hydroxybutyrate whole blood levels in mice fed *ad lib*, **(D)** bi-ventricle weights, and ventricular weight (VW)/ body weight (BW) ratio shown for male mice at 8-9 weeks of age (n = 4-5). Difference is not significant using two-tailed, unpaired t-test control vs. csBDH1$^{-/-}$.

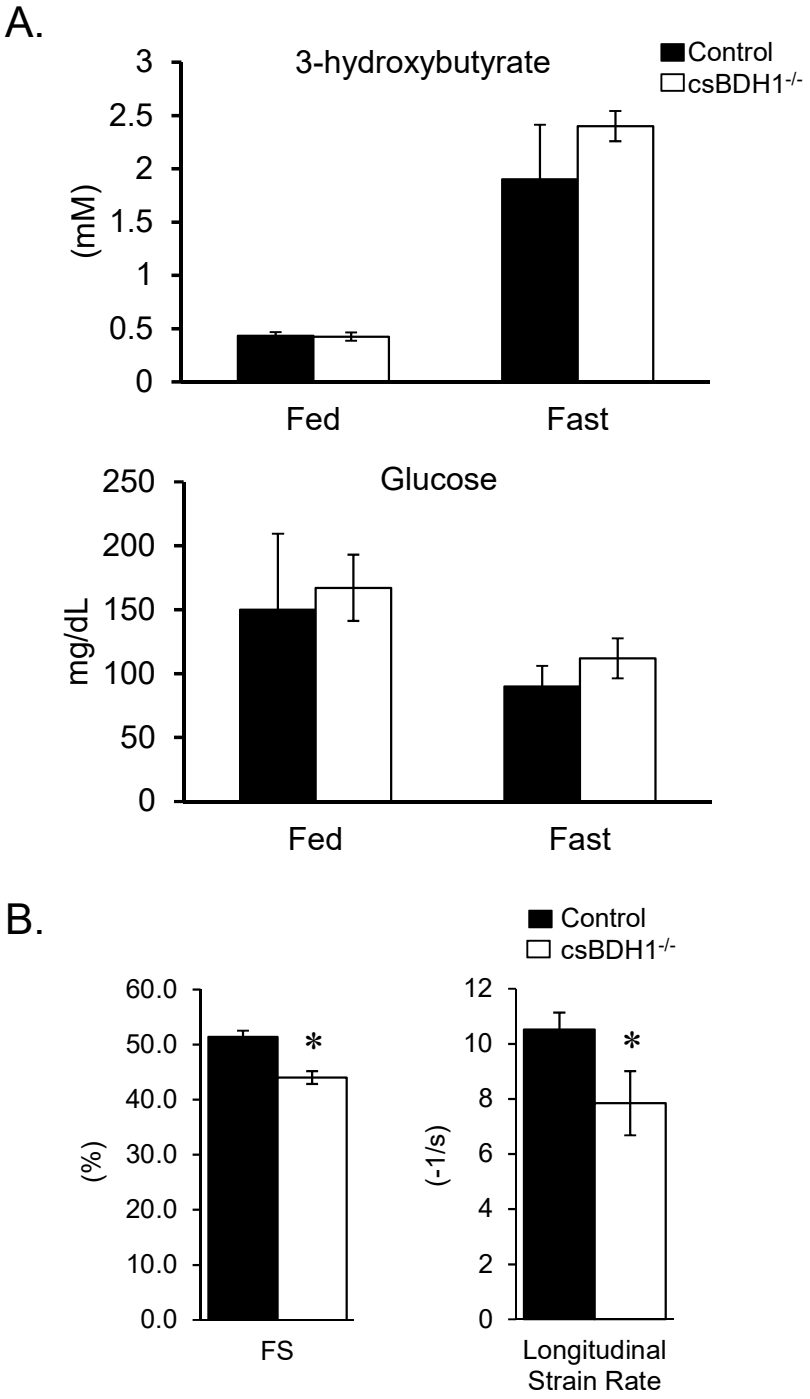

Supplemental Figure 2. Phenotype of fasted csBDH1$^{-/-}$ mice. (A) Circulating substrate levels in *ad lib* fed or 24-hour fasted control and csBDH1$^{-/-}$ male mice at 12-16 weeks of age. Top to bottom: 3-hydroxybutyrate whole blood levels and glucose levels in plasma. Bars represent mean ± SEM (n = 3-4); ns using two-tailed, unpaired t-test control vs. csBDH1$^{-/-}$. **(B)** The results of echocardiography conducted following a 24h fast of csBDH1$^{-/-}$ and control male mice aged 12-16 weeks. (Left) % Fractional shortening (FS, n=4-6) and (right) longitudinal strain rate (-1/s, n=3). All bars are shown as mean +/-SEM, *p<0.05 control vs. csBDH1$^{-/-}$ using unpaired, two-tailed t-test.

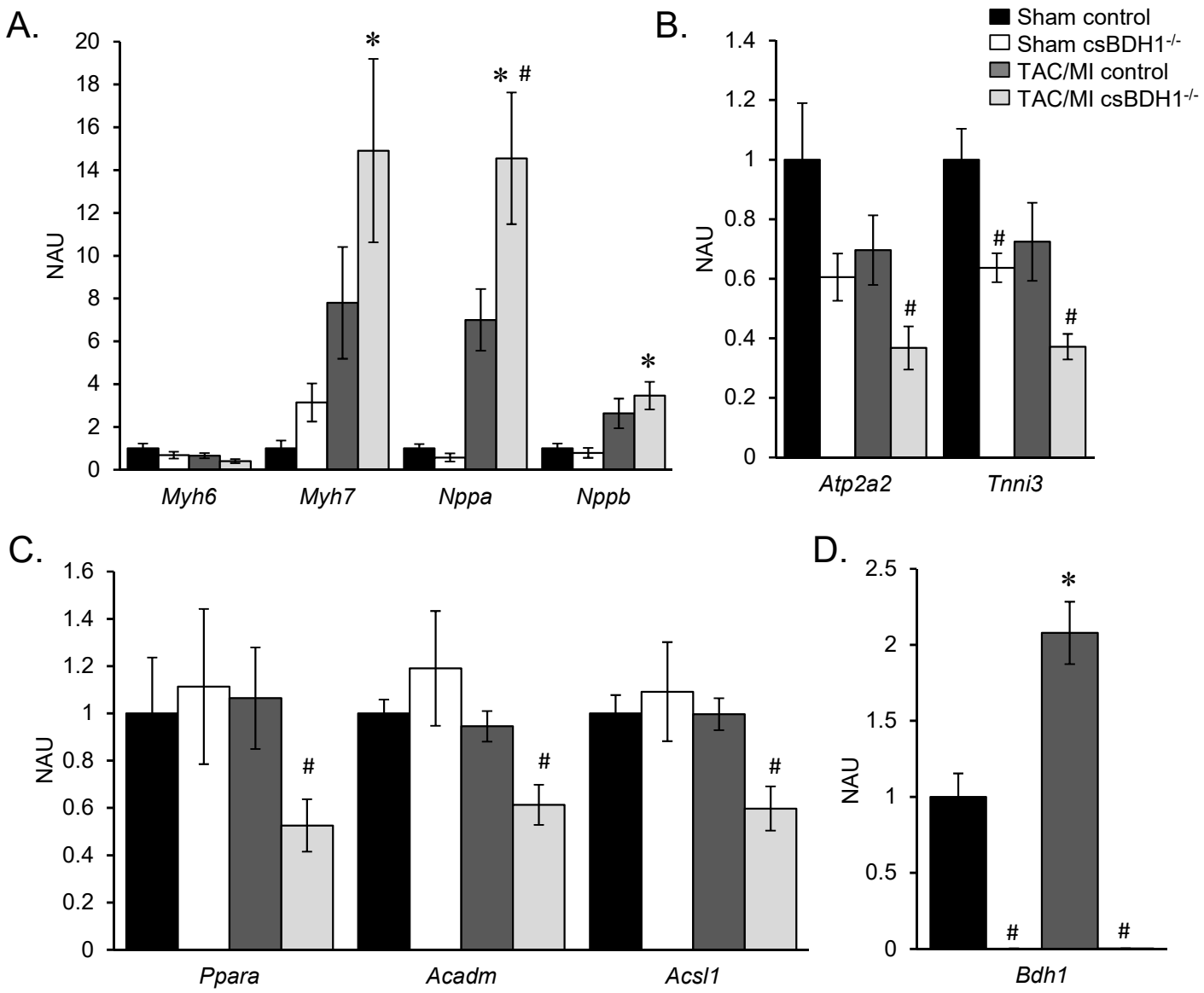

Supplemental Figure 3. Gene expression signatures indicates more severe pathological remodeling in the csBDH1$^{-/-}$ TAC/MI mice. Ventricular tissue mRNA expression levels based on qPCR for sham-operated control, sham csBDH1$^{-/-}$, TAC/MI control, and TAC/MI csBDH1$^{-/-}$ mice normalized to *Rplp0* transcript levels. **(A)** *Myh6*, *Myh7*, *Nppa*, *and Nppb* mRNA levels, **(B)** excitation-contraction coupling transcripts for *Atp2a2* and *Tnni3*, **(C)** transcript levels for energy metabolic genes including *Ppara*, *Acadm*, and *Acsl1*, and **(D)** *Bdh1* mRNA levels. Gene expression levels are shown relative to Sham WT (=1.0). Bars represent mean ± SEM (n=4-9); *p-value<0.05 Sham vs. TAC/MI; #p-value<0.05 control vs. csBDH1$^{-/-}$ using one-way ANOVA with post-hoc Fisher's LSD test. 36b4, Ribosomal Protein Lateral Stalk Subunit P0; Myh6, myosin heavy chain 6; Myh7, myosin heavy chain 7; Nppa, natriuretic peptide A; Nppb, natriuretic peptide B; Atp2a2, ATPase sarcoplasmic/endoplasmic reticulum Ca2+ transporting 2; Tnni3, Troponin I3, cardiac type; Ppara, peroxisome proliferator-activated receptor alpha; Acadm, medium-chain acyl-CoA dehydrogenase; Acsl1, long chain fatty-acid CoA ligase 1.

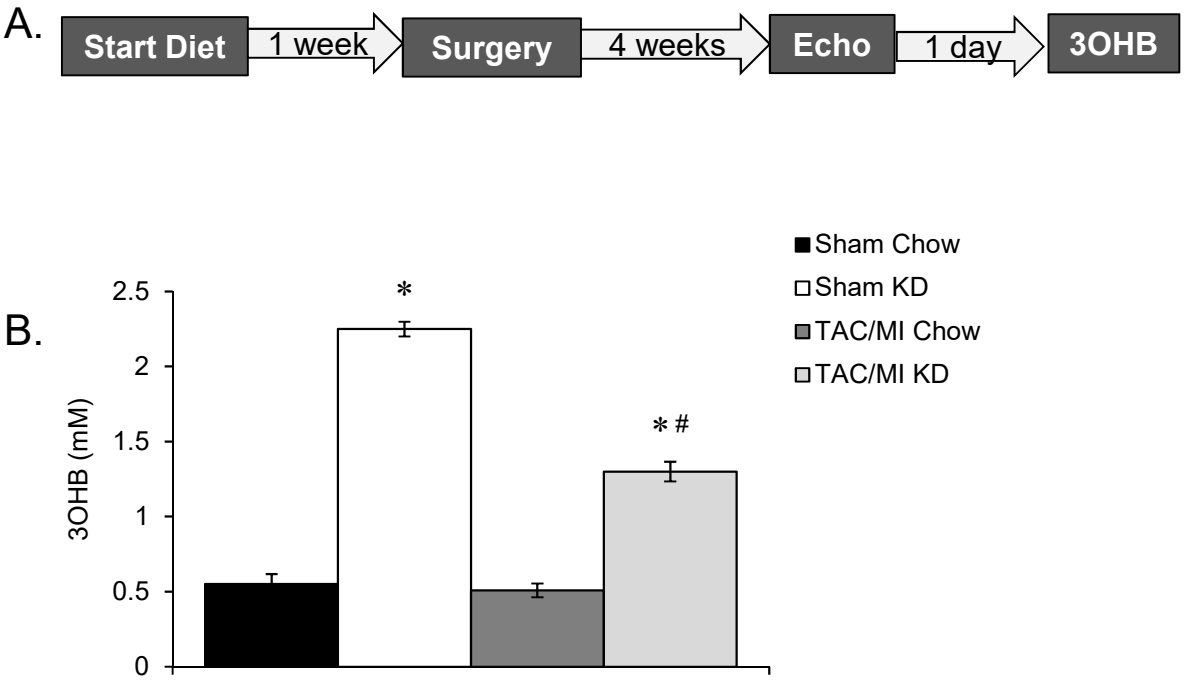

Supplemental Figure 4. Ketogenic diet results in elevated levels of circulating 3-hydroxybutyrate. Timeline of the ketogenic diet and resulting 3OHB levels for the mouse groups indicated are shown. **(A)** Mice were started on either Chow or KD 1 week before surgery. Four weeks following the surgery, echocardiographs were conducted. Mice were allowed to recover from echo for one day after which food was removed for 4 hours and circulating whole blood ketone levels were then measured. **(B)** Levels of 3OHB at time of echo are shown. Bars represent mean ± SEM (n=6-12); *p-value<0.05 Chow vs. KD or #p-value<0.05 Sham vs. TAC/MI using ANOVA with post-hoc Tukey's to correct for multiple comparisons.

Horton et al_Supplemental Figure 5

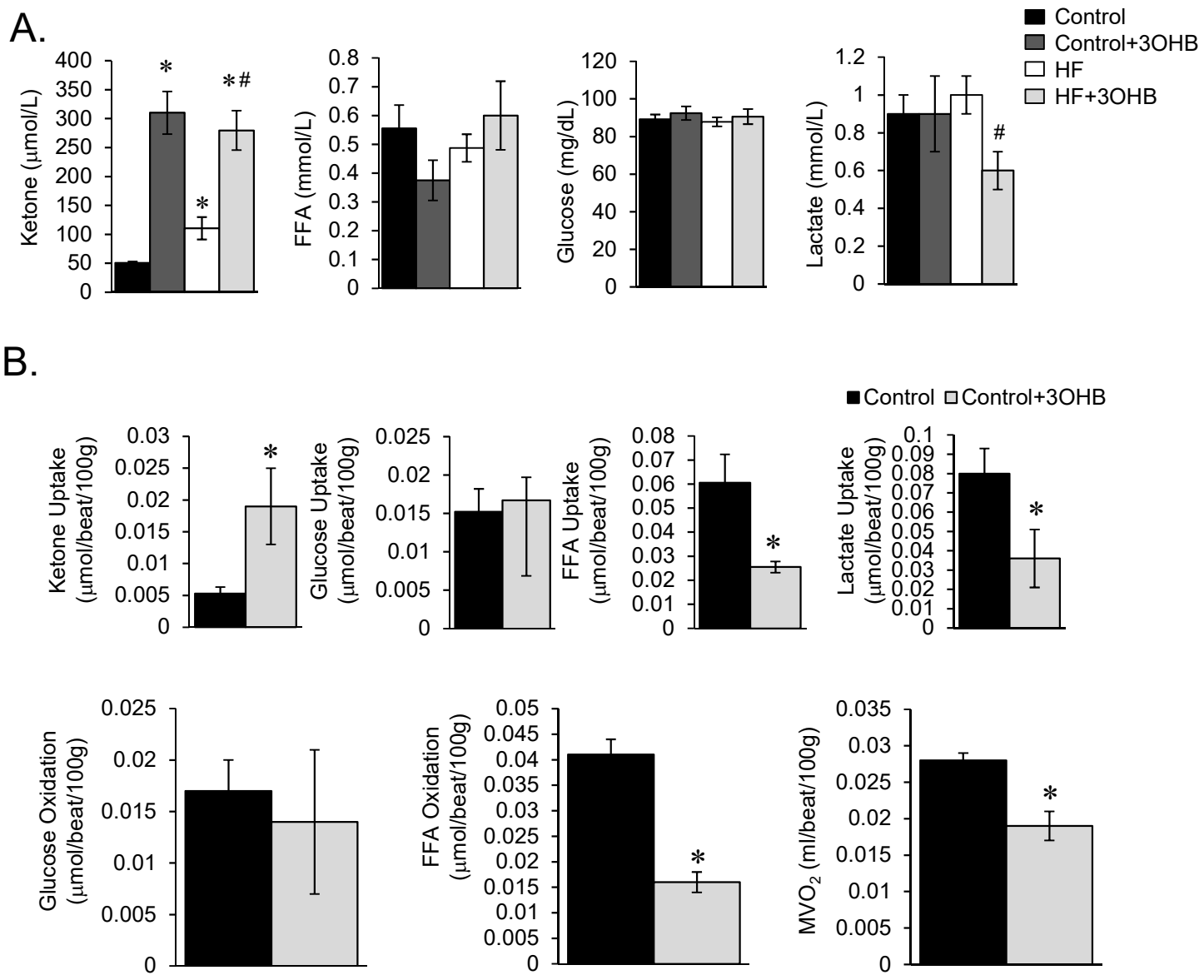

Supplemental Figure 5. Circulating levels of ketone bodies were elevated after tachypacing and further increased with 3OHB infusion. Metabolism of non-paced hearts after 3OHB infusion. (A) Arterial metabolite concentrations of (left to right) ketones, free fatty acids, glucose, and lactate measured in dogs with non-paced hearts without (Control, n=6) and with 3OHB infusion (Control+3OHB, n=5) and during the last day of cardiac pacing in dogs without (HF, n=6) and with 3OHB infusion (HF+3OHB, n=6). *p<0.05 vs. Control, or #p<0.05 HF vs. HF+3OHB one-way ANOVA followed by the Student-Newman test. The set of data for HF and non-paced controls was randomly selected from historical pools **(B)** Cardiac uptake of ketone bodies, glucose, free fatty acids (FFA), and lactate, (bottom left to right) myocardial oxidation of glucose and FFA, and myocardial oxygen consumption (MVO_2) in non-paced hearts without 3OHB infusion (Control, n=6) and with 3OHB infusion (Control+3OHB, n=5) (Top left to right) Bars represent mean ± SEM. *p<0.05 vs. Control using t-test.

Horton et al_Supplemental Figure 6

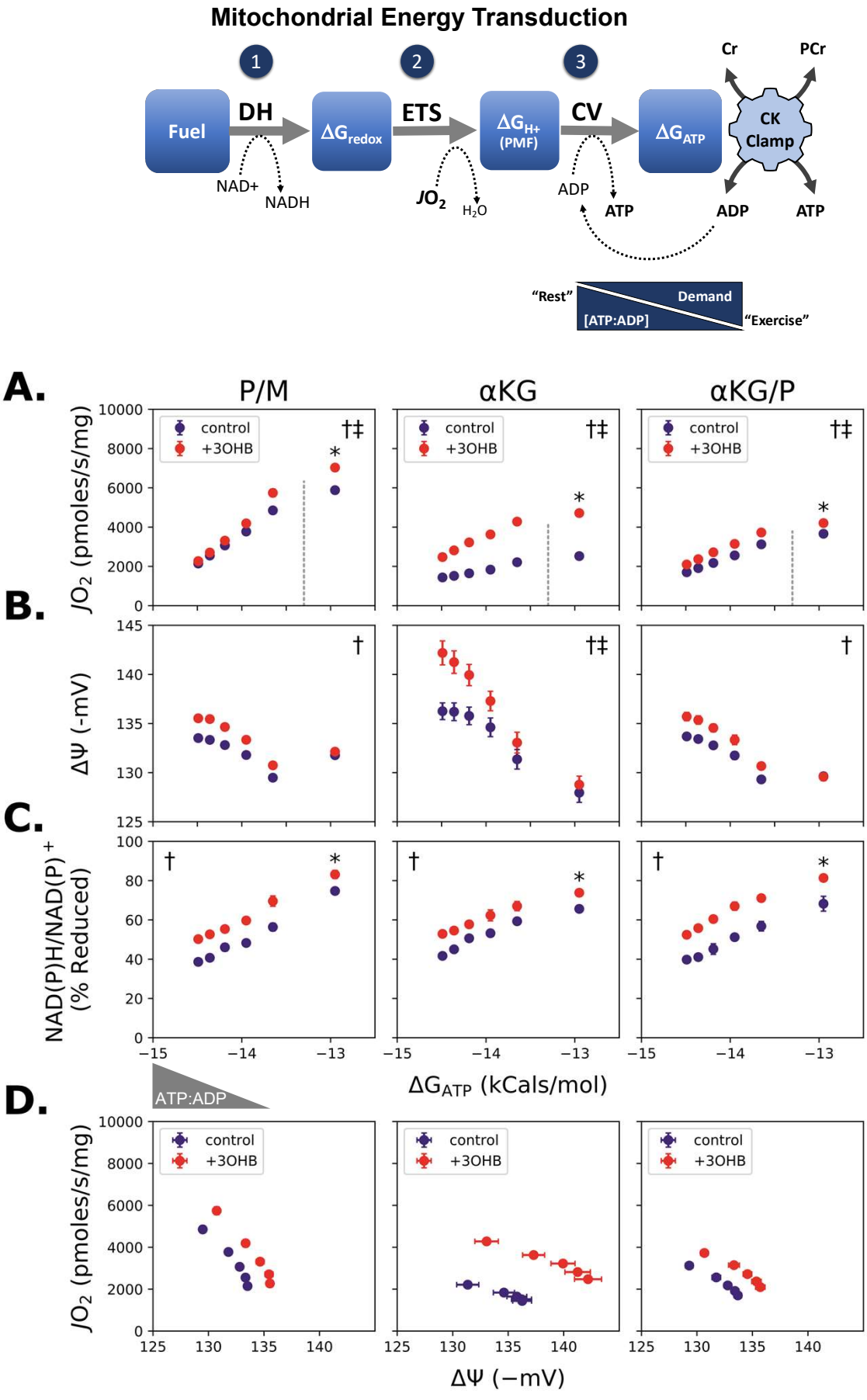

Supplemental Figure 6. 3OHB augments respiratory sensitivity and efficiency in the context of Km concentrations of anaplerotic substrates.
(**Schematic**) Mitochondrial energy transduction. The model depicts a series of inter-connected mitochondrial energy transformation steps carried out by three district control nodes whereby chemical energy present in electron-rich carbon substrates is ultimately converted to ATP free energy (ΔG_{ATP}). In Node #1 ("Matrix Dehydrogenases"), respiratory fuels activate specific dehydrogenase enzymes that convert the chemical energy available in carbon substrates to electron potential energy (ΔG_{redox}), assessed experimentally via the fluorescent measurement of the NAD(P)H/NAD(P)$^+$ redox state. Electron potential energy is then transferred to Node #2 ("Electron Transport System" (ETS)), which converts energy available in ΔG redox to proton potential energy (ΔG_{H+}) harnessed in the electrochemical proton motive force (PMF). Efficiency of energy transfer at Node 2 is assessed by fluorescent measurement of mitochondrial membrane potential (ΔΨ), the primary contributor to the PMF. In Node #3 ("ATP Synthesis"), the energy available in ΔG_{H+} drives the synthesis and transport of ATP via the ATP synthase complex (CV) and the adenine nucleotide translocase (ANT). Mitochondrial oxygen consumption (JO_2) reflects the flux of the proton current at Complex IV of the ETS and thus serves as the experimental measurement of Node #3. The assay platform used to assess respiratory sensitivity and energy transfer efficiency leverages a creatine kinase (CK) clamp technique that permits dynamic control of the energy charge (and thus energy demand) to which isolated mitochondria are exposed by titrating and maintaining the extra-mitochondrial ATP:ADP ratio within a (near) physiologic range.
(**Graphs**) Freshly isolated mitochondria from heart ventricles of C57BL/6NJ mice were utilized to assess the impact of 3-hydroxybutyrate (3OHB) on the relationship between (**A**) oxygen consumption rates (JO_2) (**B**) ΔΨ in millivolts (mV), and (**C**) NAD(P)H/NAD(P)$^+$ redox state versus the estimated Gibbs energy of ATP hydrolysis (ΔG_{ATP}). Mitochondria were energized with Km concentrations either Pyruvate + Malate (P/M; 110 μM each), α-Ketoglutarate +Pyruvate (αKG/P; 60 μM each) or α-Ketoglutarate (αKG; 550 μM) in the absence (blue) or presence (red) of 2 mM 3OHB. (**D**) Mitochondrial respiratory efficiency was evaluated by plotting JO_2 against ΔΨ m in the presence of P/M ± 3OHB, αKG/P ± 3OHB, or αKG ± 3OHB. Dotted lines separate the maximal and sub-maximal portions of JO_2 vs. ΔG_{ATP}. The right triangle illustrates the changing concentrations of ATP relative to ADP (T:D), resulting in a reciprocal change in energy demand and thus JO_2. Comparisons between ketone and vehicle control were analyzed by two-way ANOVA († = main effect of ketone, ‡ = interaction of ketone:ΔG_{ATP}, $P< 0.05$) using measurements (A-C) made at submaximal JO_2. Energy fluxes representing maximal JO_2 (ΔG_{ATP} =-12.95) were analyzed via T-test (* $P<0.05$).

Horton et al Supplemental Figure 7

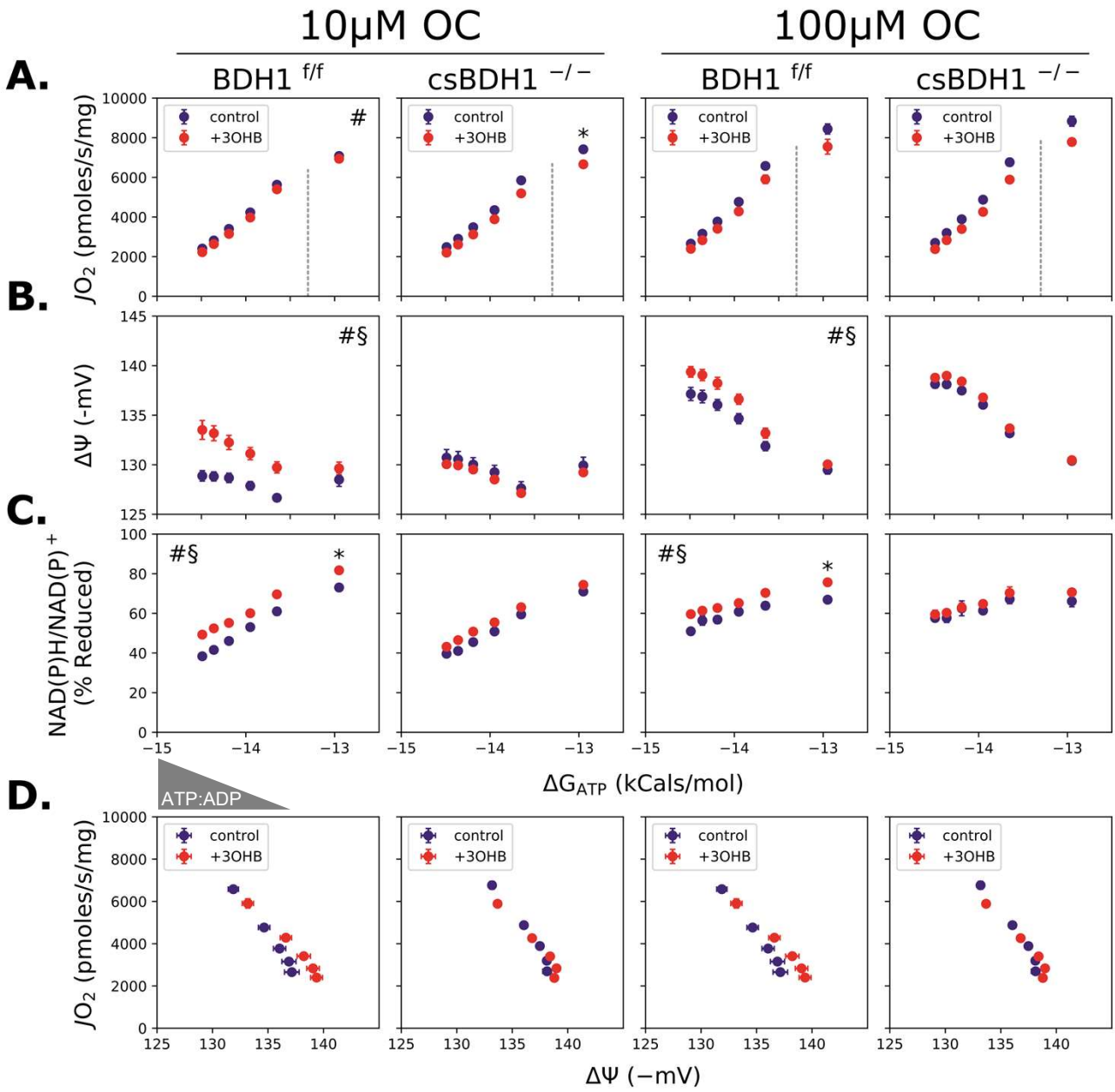

Supplemental Figure 7. The effects of 3OHB on mitochondrial respiratory efficiency require BDH1 activity. Freshly isolated mitochondria from heart ventricles of BDH1$^{fl/fl}$ controls, csBDH1$^{-/-}$ mice were utilized to assess the impact of R-3-hydroxybutyrate (3OHB) on the relationship between (**A**) oxygen consumption rate (JO_2) (**B**) mitochondrial membrane potential (ΔΨ) in millivolts (mV), and (**C**) NAD(P)H/NAD(P)$^+$ redox state versus the estimated Gibbs energy of ATP hydrolysis (ΔG_{ATP}). Mitochondria were energized with Pyruvate + Malate (P/M, 110 μM each) and L-octanoylcarnitine (OC; 10 or 100 μM) in the absence (purple) or presence (red) of 2 mM of R-3OHB. (D) Mitochondrial respiratory efficiency was evaluated by plotting JO_2 against ΔΨ. Dotted lines separate the sub-maximal and maximal portions of JO_2 vs. ΔG_{ATP}. Triangle denotes the changing concentrations of ATP relative to ADP (ATP:ADP), resulting in a reciprocal change in energy demand. Data represent mean ± SEM (N=4). Comparisons between BDH1$^{fl/fl}$ versus csBDH1$^{-/-}$ mitochondria were analyzed by three-way ANOVA followed by Tukey HSD (# ketone:genotype interaction, § ketone effect, P and FWER< 0.05) using measurements (A-C) made at submaximal JO_2. Energy fluxes representing maximal JO_2 (ΔG_{ATP} =-12.95) were analyzed by 2-way ANOVA and Tukey HSD (*FWER <0.05, relative to vehicle control).

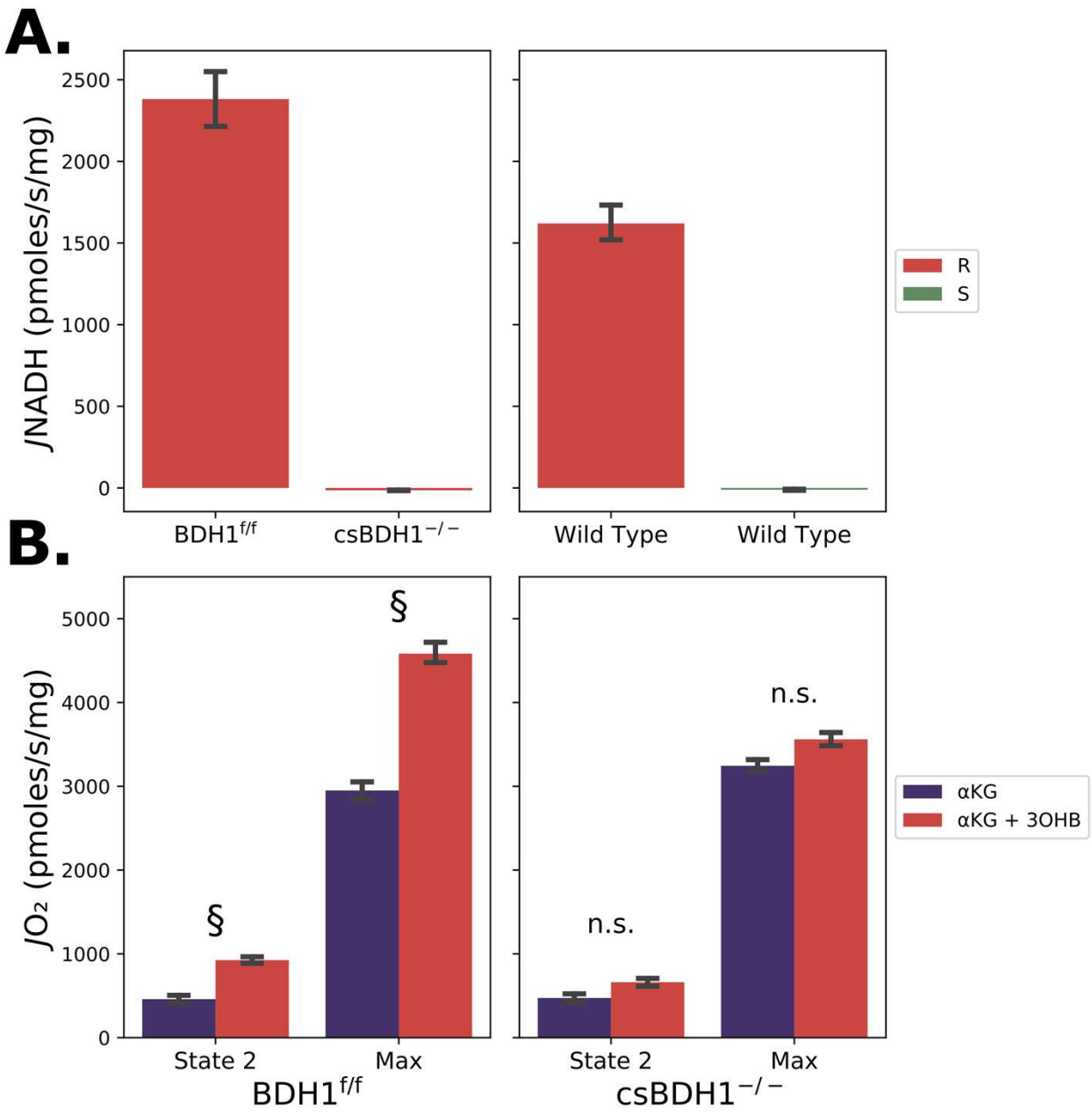

Supplemental Figure 8. The effects of 3OHB on *J*NADH and AKG-supported JO_2 require BDH1 flux. Freshly isolated mitochondria from heart ventricles of BDH1$^{fl/fl}$ controls, csBDH1$^{-/-}$ or wildtype C57BL/6N mice were (**A**) permeabilized to assess the impact of 2 mM of either the R- (R) or S- (S) enantiomers of 3OHB on rates of NADH generation (*J*NADH); or (**B**) used intact to assess rates of oxygen consumption (JO_2) in the presence of 500 μM α-Ketoglutarate (αKG) ± R-3OHB in the context of State 4 or maximal respiration during the CK clamp (estimated ΔG_{ATP} of -12.95 kcal/mole; similar to State 3). Data are presented as mean ± SEM (A, N=3) and (B, N=5). Data in B was analyzed by 3-way ANOVA (genotype x ketone x respiratory state) followed by Tukey's multiple comparisons test. (§ FWER<0.05, effect of R-3OHB versus vehicle control under specified respiratory conditions)

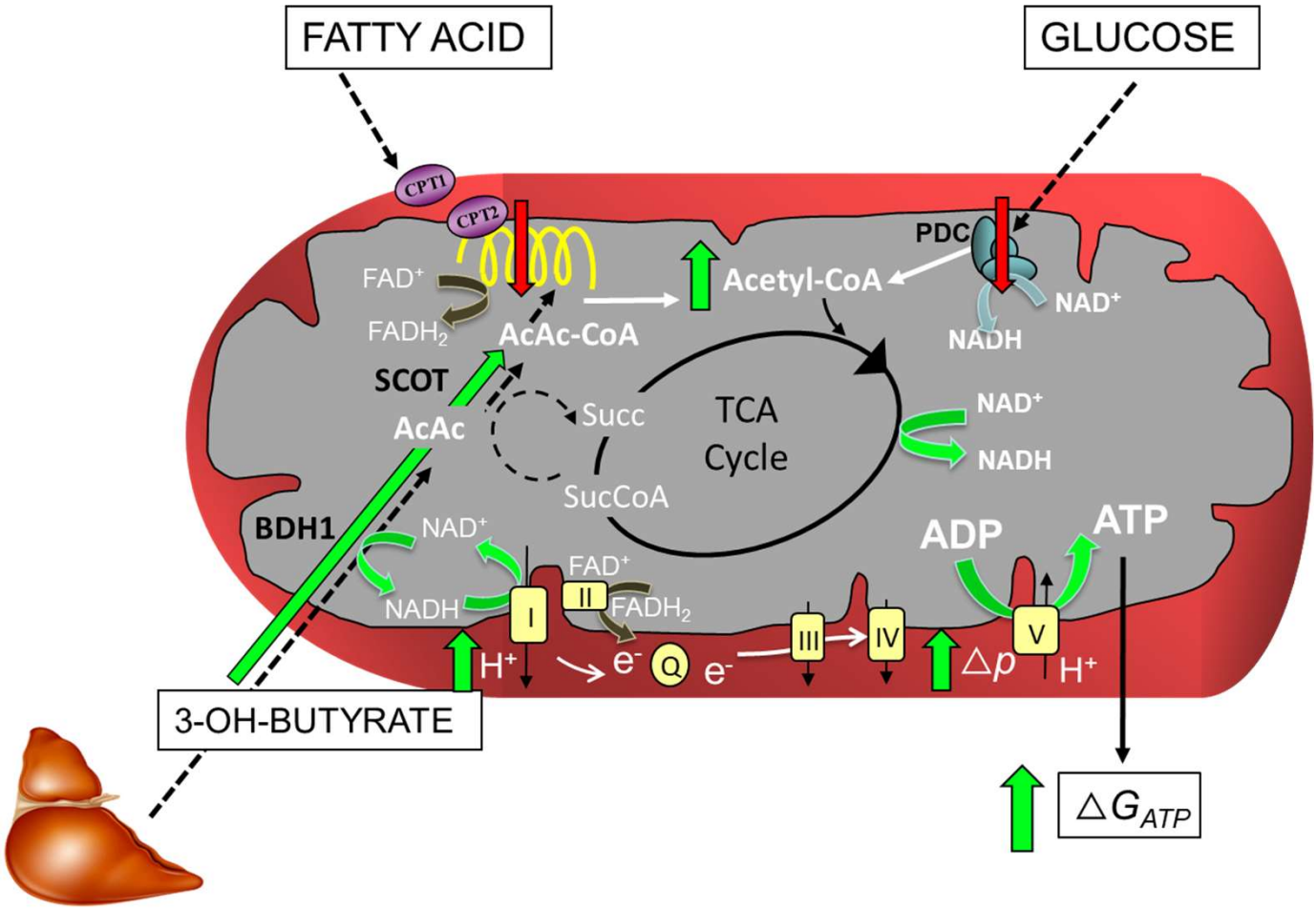

Supplemental Figure 9. Proposed impact of 3OHB on mitochondrial redox and respiratory efficiency in heart failure. Red arrows indicate reduced capacity for fatty acid (FA) and glucose oxidation contribution to the mitochondrial acetyl-CoA pool in the failing heart. Green arrows denote augmentation of acetyl-CoA pool, redox (NADH/NAD), mitochondrial membrane potential, and ATP-producing capacity secondary to increased 3-hydroxybutyrate oxidation. BHD1, beta-hydroxybutyrate dehydrogenase 1; SCOT, Succinyl-CoA:3-ketoacid CoA transferase; PDC, pyruvate dehydrogenase complex.

Supplemental Table 1. Distribution of genotypes in offspring of *Cre*$^{-/-}$, *Bdh1*$^{f/f}$ x *Cre*$^{+/-}$, Bdh1$^{f/f}$ crosses.

Male offspring at weaning				Female offspring at weaning			
Genotype	**Observations**	**Expected (%)**	**Actual (%)**	**Genotype**	**Observations**	**Expected (%)**	**Actual (%)**
Cre-/-	41	50	61	*Cre-/-*	39	50	65
Cre+/-	26	50	39	*Cre+/-*	21	50	35*

*p<0.05 expected vs. actual using chi-square analysis (n=127). BDH1, 3-hydroxybutyrate dehydrogenase 1

Supplemental Table 2. Echocardiographic analyses of csBDH1$^{-/-}$ and control mice following a 24h fast.

	Control	csBDH1$^{-/-}$
Heart rate, bpm	604.7± 14.34	624.5± 23.14
LVPWd, mm	0.874 ± 0.04	0.822 ± 0.03
IVSd, mm	0.88± 0.03	0.87 ± 0.04
LVIDd, mm	3.31± 0.09	3.77 ± 0.07*
LVPWs, mm	1.37± 0.06	1.26 ± 0.05
IVSs, mm	1.38 ± 0.05	1.29 ± 0.06
LVIDs, mm	1.61 ± 0.08	2.11 ± 0.11*
LVM, mg	98.3 ± 8.58	113.9 ± 3.01
LVMI, mg/g BW	3.75 ± 0.18	3.95 ± 0.31
RWT	0.53± 0.02	0.45 ± 0.02*
FS (%)	51.35 ± 1.43	44.03 ± 2.58*
IVCT, ms	3.01 ± 0.53	3.84 ± 0.9
ET, ms	38.72 ± 3.2	44.1 ± 2.22
IVRT, ms	13.3 ± 1.6	8.8 ± 0.6
Tei Index	0.45± 0.07	0.29 ± 0.04
ESV, μl	10.32 ± 0.3	21.19 ± 7.1
EDV, μl	37.83 ± 3.33	52.55 ± 4.68*
Radial Mean Strain %	36.95 ± 3.1	37.63 ± 1.7
Longitude Mean Strain %	21.05 ± 0.62	19.39 ± 0.85
Radial Strain Rate (1/s)	10.5 ± 1.02	10.0 ± 0.84
Longitude Strain Rate (-1/s)	10.53 ± 0.61	7.85 ± 0.66*

Values are mean +/- SEM. *p<0.05 control vs. csBDH1$^{-/-}$ using two-tailed, unpaired t-test (n=4-6 except for strain rates which are n=3-4). LVPWd, left ventricular posterior wall thickness end diastole; IVSd, Interventricular septum thickness at end-diastole; LVIDd, left ventricular internal dimension at end-diastole; LVPWs, left ventricular posterior wall thickness at end–systole; IVSs, interventricular septum thickness at end–systole; LVIDs, left ventricular internal dimension at end–systole; LVM, left-ventricular mass; LVMI, left-ventricular mass index; BW, body weight; RWT, relative wall thickness; FS, fractional shortening; IVCT, Isovolumic contraction time; ET, ejection time; IVRT, Isovolumic relaxation time; ESV, end systolic volume; EDV, end diastolic volume; EF, ejection fraction

Supplemental Table 3. Echocardiographic analyses post-TAC/MI or sham procedure in control vs. csBDH1$^{-/-}$ mice.

	Sham		TAC/MI	
	Control	csBDH1$^{-/-}$	Control	csBDH1$^{-/-}$
HR (bpm)	702.3±8.86	690.6±19.85	698±16.41	635±13.65*
BW (g)	25.96±0.79	24.96±1.05	24.6±0.36	26.3±0.64
Ao VTI Prox (mm)	3.96±0.31	3.69±0.23	3.84±0.31	3.20±0.16
Ao VTI Band (mm)	3.14±0.14	3.02±0.27	13.91±1.78	12.20±0.76
VTI Ratio	0.81±0.04	0.82±0.05	3.87±0.41	3.85±0.26
EDV (μl)	36.08±1.83	40.02±3.92	82.83±12	131.16±12*
ESV (μl)	11.94±0.79	14.23±0.86	60.69±12.22	108.46±11.77*
EF (%)	66.88±1.31	63.61±2.45	31.51±4.74	18.31±2.21*
peak velocity (mm/sec)	1.05±0.07	0.98±0.06	3.33±0.25	3.09±0.12
peak gradient (mmHg)	4.49±0.59	3.90±0.50	46.58±7.7	38.89±3.2
SWMSI	0±0	0±0	0.46±0.06	0.58±0.01

Values are mean +/- SEM (Sham, n=5-6; TAC/MI, n=9); *p<0.05 TAC/MI control vs. TAC/MI csBDH1$^{-/-}$, using unpaired, two-tailed, t-test. Cs, cardiac specific; BDH1, 3-hydroxybutyrate dehydrogenase, type 1; TAC, transverse aortic constriction; MI ,myocardial infarction; HR, heart rate; BW, body weight; Ao, aorta; Prox, proximity; VTI, velocity-time integral; EDV, end-diastolic volume; ESV, end-systolic volume; EF, ejection fraction; SWMSI, segmental wall motion score index

Supplemental Table 4. Echocardiographic analyses post-TAC/MI or sham procedure in mice fed standard chow or ketogenic diet.

	Sham		TAC/MI	
	Chow	KD	Chow	KD
HR (bpm)	707.1 ± 9.06	721.4±16.35	662±10.79	699±13.91
BW (g)	23.96±0.47	25.81±0.64	22.06±0.54	23.94±0.73
Ao VTI Prox (mm)	3.65±0.31	3.57±0.38	2.95±0.14	2.98±0.21
Ao VTI Band (mm)	3.19±0.17	3.09±0.21	18.33±1.31$^{\#}$	19.87±1.57$^{\#}$
VTI Ratio	0.90±0.05	0.92±0.09	6.49±0.62$^{\#}$	6.78±0.55$^{\#}$
EDV (μl)	42.06±4.12	37.54±3.09	123±9.47$^{\#}$	95±6.68$^{*\#}$
ESV (μl)	16.29±1.84	14.86±1.55	105±9.08$^{\#}$	78±6.79$^{*\#}$
EF (%)	60.9±2.30	60.3±2.15	15.39±1.42$^{\#}$	18.59±2.41$^{\#}$
peak velocity (mm/sec)	0.98±0.06	0.96±0.06	3.69±0.17$^{\#}$	3.71±0.20$^{\#}$
peak gradient (mmHg)	3.94±0.43	3.75±0.49	56.02±5.06$^{\#}$	56.38±6.28$^{\#}$
SWMSI	0±0	0±0	0.55±0.02$^{\#}$	0.51±0.02$^{\#}$

Mean +/- SEM is shown (n=8-15); *p<0.05 Chow vs. KD or #p<0.05 Sham vs. TAC/MI using ANOVA with Tukey's post-hoc to correct for multiple comparisons.

Supplemental Table 5. Echocardiographic analyses over time in tachypacing canine (HF) not infused with 3OHB and canines infused with 3OHB (HF+3OHB), sham controls also infused with 3OHB shown (Control+3OHB).

		Baseline	2 weeks	4 weeks
Heart Rate, bpm	HF	106.7±4.0	107.2±7.5	136.0±5.6*
	HF+3OHB	110.6±3.6	109.2±5.3	115.8±4.7 #
	Control+3OHB	111.2±6.0	114.2±9.8	-
LVSP, mmHg	HF	130.0±4.0	108.2±3.7*	91.4±3.8*
	HF+3OHB	124.3±4.0	101.5±2.9*	96.9±2.3*
	Control+3OHB	119.0±5.1	117.3±4.7	-
MAP, mmHg	HF	110.2±2.6	92.7±3.2*	77.6±3.7*
	HF+3OHB	107.0±2.0	85.1±2.8*	83.0±3.1*
	Control+3OHB	101.0±4.5	96.4±6.1	-
LVEDP, mmHg	HF	6.8±1.2	10.5±1.5	25.3±0.6*
	HF+3OHB	6.1±0.6	9.6±2.0	8.2±1.2 #
	Control+3OHB	3.6±2.0	6.4±1.7	-
dp/dt_{max}, mmHg/s	HF	3776±260	2002±249*	1533±102*
	HF+3OHB	3975±461	2575±486*	1840±98*
	Control+3OHB	3340.0±708	2922±204	-
dp/dt_{min}, mmHg/s	HF	-3168±194	-2284±76*	-1905±125*
	HF+3OHB	-3178±422	-2437±315*	-1901±94*
	Control+3OHB	-2558±220	-2773±142	-
MCBF, ml/min	HF	57.9±1.2	53.0±5.1	56.9±1.5
	HF+3OHB	59.1±5.8	51.1±3.8	62.5±2.8
	Control+3OHB	61.5±2.2	53.3±3.8	-
Ea, mmHg/ml	HF	4.3±0.4	4.4±0.4	4.2±0.4
	HF+3OHB	4.2±0.2	4.2±0.4	3.4±0.2*
	Control+3OHB	4.2±0.5	3.5±0.5	-
TPR, mmHg/L	HF	41.1±6.4	37.2±3.3	44.6±4.3
	HF+3OHB	36.2±2.6	32.2±2.9	26.8±1.8*#
	Control+3OHB	38.3±4.9	32.6±6.6	-
LVEF, %	HF	64.3±1.8	51.3±2.3*	37.0±3.1*
	HF+3OHB	66.9±3.4	58.9±2.2*	56.1±1.5*#
	Control+3OHB	69.8±2.9	68.2±2.6	-
LVEDD, mm	HF	42.0±1.2	44.9±1.7*	50.1±1.2*
	HF+3OHB	40.4 ±0.4	43.9±0.5*	45.4 ±0.8*#
	Control+3OHB	40.5±0.5	41.2±0.2	-
CO, L/min	HF	3.1±0.4	2.5±0.2	1.9±0.2*
	HF+3OHB	2.9±0.3	2.7±0.2	3.2±0.2#
	Control+3OHB	2.7±0.2	3.2±0.5	-

LVSP, LV systolic pressure; MAP. Mean arterial pressure; LVEDP, LV end-diastolic pressure; MCBF, mean coronary blood flow; Ea, effective arterial elastance; TPR, total peripheral resistance; LVEF, LV ejection fraction; LEDD, left ventricular end-diastolic diameter; CO, cardiac output. The set of data for HF was randomly selected from historical pools. *P<0.05 vs baseline; # P<0.05 3OHB vs HF.

SUPPLEMENTAL METHODS

Mouse Cardiac Surgery and echocardiography

Transverse aortic constriction (TAC) was performed on anesthetized mice by first freeing the aortic arch by blunt dissection. A 7-0 silk suture was passed under the aorta. The suture was then tied around a blunt needle (25 to 28 gauge depending on size of animal) lying on the artery, and the blunt needle was removed to induce constriction. Second, to generate a small myocardial infarction (MI), the chest wall was retracted through the 4th intercostal space to clearly visualize the left ventricle and the left anterior descending artery. The left anterior descending branch (LAD) of the left coronary artery was ligated with a 9-0 nylon suture.

Ultrasound examination of the cardiovascular system was non-invasively performed using a Vevo2100 Ultrasound System (VisualSonics Inc, Toronto, Ontario, Canada). Mice have cursory examination of cardiac structure and function under physiologic conditions obtained by hand-held manipulation of the ultrasound transducer (30-60 MHz). The detailed ultrasound examination was performed with animals secured on an imaging platform in supine position using isoflurane (3% induction and 1.5% maintenance) through a customized nose cone. Physiologic parameters including heart rate, respiratory rate, and core body temperature were continuously monitored by a built-in monitoring system. Complete two-dimensional, M-mode, and Doppler ultrasound examinations were performed using multiple views.

Metabolite Measurements

Briefly, a 50 µL aliquot of heart tissue homogenate on ice was spiked with a 10 µL mixture of isotopically-labeled internal standards (sodium L-lactate-3,3,3-d_3, sodium pyruvate-$^{13}C_3$, sodium D-3-hydroxybutyrate-1,3-$^{13}C_2$, succinic-$^{13}C_4$ acid, fumaric-$^{13}C_4$ acid, L-malic-$^{13}C_4$ acid, alpha-

ketoglutaric acid disodium salt (1,2,3,4-$^{13}C_4$), and citric-2,2,4,4-d_4 acid; Sigma-Aldrich, St. Louis, MO, Cambridge Isotopes, Cambridge, MA, and CDN Isotopes, Quebec, Canada). This was followed by the derivatization of organic acids with of 50 µL of 0.4 M O-benzylhydroxylamine and 10 µL of 2 M 1-ethyl-3-(3-dimethylaminopropyl)carbodiimide at room temperature for 10 min. The derivatized organic acids were extracted from the homogenate by liquid–liquid extraction using 100 µL of water and 600 µL of ethyl acetate. Samples were briefly vortexed and centrifuged at 18,000g for 5 min at 10 °C. A 100 µL aliquot of the ethyl acetate layer was dried under nitrogen and reconstituted in 1 mL of 50/50 methanol/water prior to LC/MS/MS analysis. Derivatized organic acids were separated on a 2.1 x 100 mm, 1.7 µm Waters Acquity UPLC BEH C18 column (T = 45 °C) using a 7.5 min. linear gradient with 0.1% formic acid in water and 0.1% formic acid in acetonitrile at a flow rate of 0.3 mL/min. Quantitation of derivatized organic acids was achieved using multiple reaction monitoring on a Thermo Scientific UltiMate 3000 HPLC/Quantiva triple quadrupole mass spectrometer (Thermo Scientific). Standard calibration curves for derivatized organic acids were prepared by spiking 10 µL aliquots of organic acids (Sigma-Aldrich) and internal standards (Sigma-Aldrich; Cambridge Isotopes; CDN Isotopes) into 50 µL aliquots of a 50/50 acetonitrile/0.3% formic acid solution. Calibration samples were derivatized and extracted similarly to the organic acids above.

Substrate Kinetics

Substrate kinetic assays were performed using high resolution respirometry (Oroboros Oxygraph-2K (Oroboros Instruments)) at 37°C in a 2 mL reaction volume of Buffer D supplemented with glucose (5 mM) and hexokinase (1 U/mL, Sigma H4502) to clamp the ADP

concentration and prevent ATP accumulation. Following addition of isolated mitochondria (0.025 mg/mL), and then adenosine diphosphate (ADP, 2.5 mM), substrates were added sequentially to titrate the concentration from 10 μM to 10 mM and included α-ketoglutarate; pyruvate and malate; and α-ketoglutarate and pyruvate. For the combined substrate conditions, equal concentrations of both metabolites were used. Steady-state JO_2 was plotted as a function of substrate concentration. A non-linear fit of the Michaelis-Menten equation was performed using GraphPad Prism version 7.04 for Windows to determine the Michaelis constant (Km) for the substrates: 110 μM pyruvate and malate; 550 μM α-ketoglutarate; 60 μM α-ketoglutarate and pyruvate, which were used subsequently for assays involving the creatine kinase clamp.

BDH1 Activity

Briefly, activity buffer consisted of buffer D supplemented with alamethicin (30 μg/mL), rotenone (5 μM) and NAD+ (2 mM). In a 96 well plate, 200 μL of assay buffer was added per well, followed by isolated mitochondria. The assay performed at 37°C and was initiated by the addition of enzymatic substrate (10 mM R-3-Hydroxybutyric acid or S-3-Hydroxybutyric acid). NADH production was monitored via autofluorescence (Ex:Exm 340/450 nm). Fluorescent units were converted to pmoles of NADH via standard curve.